Proceedings of the 17th World Congress
The International Federation of Automatic Control
Seoul, Korea, July 6-11, 2008

Real-time Monitoring of Thin Film Microstructure in Chemical Vapor Deposition using a Modified Moving Horizon Estimation ⋆

Rentian Xiong * **Martha Grover Gallivan** **

* *School of Chemical & Biomolecular Engineering, Georgia Institute of Technology, Atlanta, GA, 30332-0100 USA (Tel: 404-894-3030; e-mail: rxiong@chbe.gatech.edu)*
** *School of Chemical & Biomolecular Engineering, Georgia Institute of Technology, Atlanta, GA, 30332-0100 USA (Tel: 404-894-2878; e-mail: martha.gallivan@chbe.gatech.edu)*

Abstract: A modified moving horizon estimator (mMHE) was proposed to estimate thin film thickness, growth rate, surface roughness and refractive indices *in situ* from a dual-wavelength reflectance measurement during chemical vapor deposition (CVD). mMHE was compared with the commonly used recursive least squares fitting (RLS) method in both simulated and experimental CVD processes. The results indicate that mMHE yielded more accurate estimates than RLS by incorporating the *a priori* estimate in the objective function.

Keywords: chemical vapor deposition; moving horizon estimation; microstructure.

1. INTRODUCTION

Chemical vapor deposition (CVD) is an industrially important process with a wide range of applications such as IC fabrication, optical, and thermal coatings (Pierson [1999]). Because the applications are largely dependent on the microstructure of the deposited film (e.g. thickness and roughness), it is highly desirable to control the microstructure during the deposition. The control of film microstructure has motivated research efforts on *in situ* sensing for CVD processes (Buzea and Robbie [2005]). Currently optical sensors like the reflectometer and ellipsometer are the most common because they are compatible with the processing environment of CVD, which involves high temperature, low pressure and reactive materials. The challenge of optical sensors is that film microstructure is not measured directly and must be extracted from the indirect optical measurement.

Various techniques have been reported to interpret the *in situ* sensor data (Breiland and Killeen [1995], Balmer et al. [2002], Stafford et al. [1998], Comina et al. [2005]). The simplest method is recursive least squares fitting (RLS). In RLS, film parameters such as growth rate and refractive index are assumed to be constant in a fixed window and are estimated by minimizing the square of the error between the sensor model prediction and the measurement. When new measurement data is acquired, the window is shifted to include new data and to discard part of the old data. The optimal solution in the previous window is passed into the new window as an initial guess for the fitting. RLS usually assumes a smooth film surface so that a simple optical model can be used. In practice, however, the film surface may be rough depending on the processing conditions and the resulting microstructure. The roughness can affect reflectance by scattering the light. There are some reports on extracting surface roughness from reflection measurements with limited success (Luo et al. [2002], Zuiker et al. [1996]). In addition, RLS does not use the *a priori* knowledge of the film microstructure to compute the new estimate. The sensor model is highly nonlinear and the error surface contains multiple local minima. Without the *a priori* knowledge, the parameters may get caught in these local minima.

One solution is to put constraints on the fitted parameters. A more rigorous approach is to include the *a priori* state estimates in the objective function. The framework of this more general least squares fitting is provided by the moving horizon estimator (MHE) (Robertson and Lee [1995], Robertson et al. [1996], Rao et al. [2001, 2003], Haseltine and Rawlings [2005]). MHE considers the error not only from the sensor model, but also from the process model and the *a priori* estimate. In addition, MHE explicitly considers uncertainty and the correlations between fitted parameters. This is highly desirable when estimating parameters that are highly correlated, such as film thickness and refractive index, or surface roughness and film absorption. Xiong and Gallivan used MHE to extract film growth rate, thickness and refractive index of yttrium oxide film on silicon substrate from a single-wavelength *in situ* normal reflectance measurement (Xiong and Gallivan [2007]) and obtained more accurate results compared to a simple least squares fitting method. The disadvantage

⋆ This work was supported by the National Science through CAREER grant *A Systems Approach to Materials Processing* and by the Georgia Tech Foundation.

of MHE, however, is that it is computationally expensive, which limits online implementation.

In this paper a modified moving horizon estimator (mMHE) is proposed to address the computational issues of MHE. The idea is to assume a deterministic process model so that only the initial state, instead of all states in the window, has to be estimated. In mMHE the objective function consists only of sensor model error and error from the *a priori* estimate. We first compare mMHE with RLS in a simulated film growth process in which the film growth rate and surface roughening rate decrease slowly. We then compare them on our CVD testbed where a yttrium oxide film was deposited on a silicon substrate. The estimated film thickness, roughness and refractive indices were compared with *ex situ* ellipsometry and AFM characterization. In a previous paper (Xiong et al. [2006]) we applied the extended Kalman filter to the reflectance data, while this paper focuses on the currently used least squares fitting method, and the ability of the prior estimate to improve upon that approach.

2. ALGORITHM

Consider a thin film deposition process with an *in situ* dual-wavelength (λ_1 and λ_2) reflectance measurement. The discrete state-space model can be written as

$$\begin{bmatrix} h \\ G \\ h_e \\ G_e \\ n_{f1} \\ n_{f2} \end{bmatrix}_{k+1} = \begin{bmatrix} h + G \times \Delta t \\ G \\ h_e + G_e \times \Delta t \\ G_e \\ n_{f1} \\ n_{f2} \end{bmatrix}_{k} + w_k \tag{1}$$

$$y_k = g\left(\begin{bmatrix} h \\ h_e \\ n_{f1} \\ n_{f2} \end{bmatrix}_k \right) + v_k \tag{2}$$

where h, G, h_e,G_e, n_{f1} and n_{f2} are thickness, growth rate, effective medium layer (EMA) thickness, EMA growth rate, and refractive index of the film at wavelength λ_1 and λ_2, respectively. The effective medium layer is commonly used to model surface roughness (Carniglia and Jensen [2002]). Eq. (1) is referred to as the process model f. As shown, h and h_e are simply the integration of G and G_e with time. G, G_e, n_{f1} and n_{f2} are assumed constant. w represents uncertainty of the process model and is assumed to be zero-mean and with a Gaussian distribution. The function g in Eq. (2) is the sensor model. $y \in \mathbb{R}^2$ is the model prediction (reflectance at λ_1 and λ_2). $v \in \mathbb{R}^2$ represents the uncertainty of the sensor model and is also assumed to be zero-mean and Gaussian. The sensor model is based on light interference on a three-layer structure which consists of substrate, film and effective medium layer. The sensor model can be derived from (Crook [1948]) and is shown in Eq. (3):

$$y = \left| \frac{r_{01} + r_{12}\exp(-j\varphi_1) + r_{23}\exp(-j(\varphi_1+\varphi_2))}{1 + r_{01}r_{12}\exp(-j\varphi_1) + r_{01}r_{23}\exp(-j(\varphi_1+\varphi_2))} \frac{+r_{01}r_{12}r_{23}\exp(-j\varphi_2)}{+r_{12}r_{23}\exp(-j\varphi_2)} \right|^2 \tag{3}$$

where $\varphi_1 = 4\pi n_e h_e/\lambda$, $\varphi_2 = 4\pi n_f h/\lambda$, n_e and n_f are the refractive indices of EMA and the film, respectively. r_{01}, r_{12} and r_{23} are the complex reflectance at the interface between vacuum and EMA, between EMA and the film, and between the film and the substrate, respectively. $r_{01} = \frac{1-n_e}{1+n_e}$,$r_{12} = \frac{n_e-n_f}{n_e+n_f}$ and $r_{23} = \frac{n_f-n_s}{n_f+n_s}$. n_s is the refractive index of the substrate, and n_e is the effective refractive index of the EMA layer, where $n_e^2 = (1+n_f^2)/2$.

2.1 Modified moving horizon estimator (mMHE)

The algorithm of the general moving horizon estimator can be found in (Robertson and Lee [1995], Robertson et al. [1996], Rao et al. [2001, 2003], Haseltine and Rawlings [2005]). The difference of mMHE is that the process model is deterministic so that only the initial state in the moving window needs to be estimated. With the above state-space model, given a sequence of measurements in a window starting from $k-m+1$ to k, mMHE estimates the states in the window by solving the following minimization problem:

$$\min_{x_{k-m+1}} \left[(x^e_{k-m+1})^T P^{-1}_{k-m+1|k-m} x^e_{k-m+1} + \sum_{l=k-m+1}^{k} v_l^T R^{-1} v_l \right] \tag{4}$$

s.t.

$$x^e_{k-m+1} = x_{k-m+1} - x_{k-m+1|k-m}$$
$$v_l = y_l - g(f^{l-(k-m+1)}(x_{k-m+1}))$$

As shown, the objective function consists of two error terms. The first term, x^e_{k-m+1}, is the error between the initial state x_{k-m+1} and the *a priori* estimate $x_{k-m+1|k-m}$. The term $x_{k-m+1|k-m}$ denotes the estimate at time $k-m+1$ based on the measurements up to time $k-m$. $P_{k-m+1|k-m}$ is the covariance matrix of the *a priori* estimate. The inverse of $P_{k-m+1|k-m}$ is used as a weighting matrix for x^e_{k-m+1} in the objective function. The second term, $v_l = y_l - g(x_l)$, is the error between the measurement and sensor model prediction. R is the covariance matrix of the sensor model uncertainty, v. The inverse of R is used as a weighting matrix for v in the objective function. When new measurement data is acquired, MHE shifts the window to include the new data and discard some of the old data. This is necessary to prevent the minimization problem from growing in size without bound. When the window shifts, *a priori* knowledge about the initial state $x_{k-m+2|k-m+1}$ and its covariance matrix $P_{k-m+2|k-m+1}$ must be updated so that the information obtained in the previous window can be passed into the current window. A common update scheme is to use the extended Kalman filter (EKF) algorithm (Robertson et al. [1996]).

The update scheme for $x_{k-m+2|k-m+1}$ and $P_{k-m+2|k-m+1}$ using EKF is shown in Eq. (5) and (6). The measurement-correction terms of EKF are

$$\begin{aligned} L_{k-m+1} &= P_{k-m+1|k-m} C^T_{k-m+1|k} \\ &\quad (C_{k-m+1|k} P_{k-m+1|k-m} C^T_{k-m+1|k} \\ &\quad + R)^{-1} \\ x_{k-m+1|k-m+1} &= x_{k-m+1|k-m} \\ &\quad + L_{k-m+1}[y_{k-m+1} - g(x_{k-m+1|k}) \end{aligned} \tag{5}$$

$$-C_{k-m+1|k}(x_{k-m+1|k-m} - x_{k-m+1|k})]$$

$$P_{k-m+1|k-m+1} = (I - L_{k-m+1}C_{k-m+1|k})P_{k-m+1|k-m}$$

The measurement-prediction terms of EKF are

$$x_{k-m+2|k-m+1} = f(x_{k-m+1|k}) + A_{k-m+1|k}(x_{k-m+1|k-m+1} - x_{k-m+1|k}) \quad (6)$$

$$P_{k-m+2|k-m+1} = A_{k-m+1|k}P_{k-m+1|k-m+1}A^T_{k-m+1|k} + Q$$

where $C_{k-m+1|k} = \frac{\partial g(x)}{\partial x}\Big|_{x=x_{k-m+1|k}}$.

2.2 Recursive least squares (RLS)

RLS is a special case of mMHE when only the error between the sensor model prediction and measurement is considered. The minimization problem in RLS is shown in Eq. (7)

$$\min_{x_{k-m+1}} \sum_{l=k-m+1}^{k} v_l^T R^{-1} v_l \quad (7)$$

s.t.

$$v_l = y_l - g(f^{l-(k-m+1)}(x_{k-m+1}))$$

where $f^{l-(k-m+1)}(x_{k-m+1})$ denotes process model f was applied $l-(k-m+1)$ times on x_{k-m+1} to calculate x_l. Once x_{k-m+1} is estimated, other states in the window can be reconstructed through process model f. Because RLS does not utilize the *a priori* estimate, it does not have much control over the optimization. On the other hand, mMHE allows users to tune the weighting matrices $P_{1|0}$, Q, and R to obtain an improved estimate.

3. SIMULATION

A simulated thin film deposition process with slowly decreasing growth rate and surface roughening rate was used to compare the performance of RLS and mMHE. The process model used to generate the data is shown in Eq. (8).

$$\begin{bmatrix} h \\ G \\ h_e \\ G_e \\ n_1 \\ n_2 \end{bmatrix}_{k+1} = \begin{bmatrix} h + G \times \Delta t \\ G \times 0.99 \\ h_e + G_e \times \Delta t \\ G_e \times 0.99 \\ n_1 \\ n_2 \end{bmatrix}_k + w_k \quad (8)$$

The sensor model is the same as Eq. (2). The wavelengths are $\lambda_1 = 950$ nm and $\lambda_2 = 470$ nm. The substrate refractive index are those of silicon at 500°C and equal to 3.7687-0.0281j and 4.8438-0.1528j at 950 nm and 470 nm, respectively (Jellison and Burke [1986], Jellison and Modine [1994]). The extinction coefficients of the film are fixed and equal to 1×10^{-3} and 2×10^{-2} for 950 nm and 470 nm, respectively. It would be possible to also estimate these parameters, although for yttria they are negligible at room temperature and very small at high temperature. We note that both h_e and k cause a decay in the reflectance amplitude, and thus their estimates would be highly correlated.

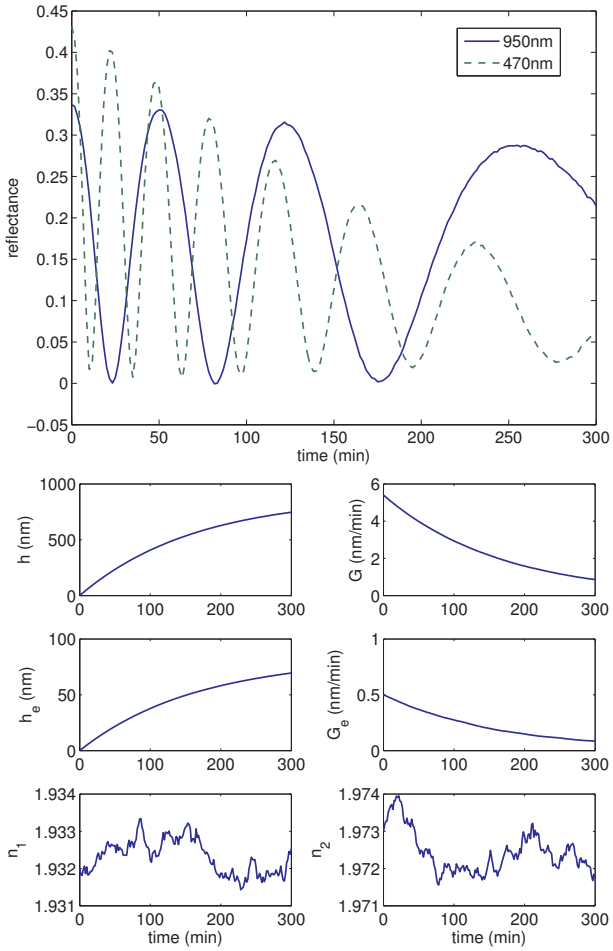

Fig. 1. Simulated film deposition process. (top) measurements (bottom) states.

The initial state is $x_i = [0\ 5.4\ 0\ 0.5\ 1.9320\ 1.9730]^T$. The covariance matrices are $\text{diag}(x_i) \times 10^{-8}$ and $\text{eye}(2) \times 10^{-6}$ for the process model and the sensor model, respectively, which are quite low. eye(2) denotes a 2×2 identity matrix. The time interval is $\Delta t = 100$ seconds, and the total deposition time is 300 minutes. The simulated measurement and states are shown in Fig. 1. The oscillation of the reflectance is due to light interference. The oscillation period gradually increases due to the decrease of growth rate. The decrease of the amplitude of oscillation is due to light scattering caused by surface roughness.

mMHE and RLS were used to extract states from the simulated measurement. The process model used in estimation is Eq. (1) which assumes a constant growth rate and surface roughening rate. The question here is whether or not mMHE and RLS can adapt to estimate the film properties when the process model is incorrect. The sensor model is the same as Eq. (2). Substrate refractive indices and film extinction coefficients are assumed known. The initial guess of film parameters is 10% offset from the real state, i.e. $x_1 = [0\ \ 5.4\ \ 0\ \ 0.5\ \ 1.9320\ \ 1.9730]^T \times 1.1$.

All states were constrained to be positive. For mMHE, there are three additional tuning parameters, i.e. $P_{1|0}$, the initial covariance matrix for x_1, the covariance matrix for the sensor model uncertainty R, and the covariance matrix for the process model uncertainty Q. In this example, $P_{1|0} = \text{diag}(x_1 \times 0.1) \times 10^2$, $R = \text{eye}(2) \times 10^{-2}$ and $Q = \text{diag}(x_1 \times 0.1) \times 10^{-2}$. $\text{diag}(x_1 \times 0.1)$ denotes that the variance of each state is 10% of its initial value. 10^2 and 10^{-2} are scaling factors to scale the covariance matrices. In this simulation study, we know the sensor model is accurate and the initial guess is not. Therefore we used large $P_{1|0}$ and small R to indicate their relative importance. Note that Q and R do not directly correspond to the noise levels used in the simulation for v_k and w_k. Q and R should be higher, because they also account for unmodeled effects such as the drifting growth rate.

The estimated results are shown in Fig. 2. As shown, the estimates by RLS are quite oscillatory and mMHE yielded a more accurate estimate than RLS with the same measurement and initial guess due to the incorporation of the *a priori* estimate. Initially P was set large so that in Eq. (4) the weighting matrix of x_1^e is very small and the *a priori* x_1 estimate is neglected when solving the minimization problem. This is essentially the same as RLS. However, after the first window, P was updated by EKF. If a good fit was obtained in the first window, P should become small to indicate more confidence on the *a priori* estimate for the next window. Then in the next window, the optimization algorithm weights more on the *a priori* estimate and limits the change of the parameters. In RLS, however, the *a priori* estimate was not used in the objective function and this is equivalent to not updating the covariance matrix P. Because of this the solution of RLS in Fig. 2 oscillates more between windows, especially for longer m since the process is changing over this window. Figure 3 shows the evolution of variance of each state in mMHE. As expected, the variance of growth rate, roughening rate and refractive indices are large initially but quickly dropped because of the EKF update due to the good fit of the measurements. The variance of thickness and roughness are large because they are the integration of growth rate and roughening rate. Therefore the error was amplified through the process model. It is an additional advantage of mMHE to explicitly consider the covariance matrix P because it computes the confidence on the estimate and also the correlations between states.

4. EXPERIMENTAL

mMHE and RLS were also compared in an experimental CVD testbed where a polycrystalline yttrium oxide thin film was deposited on a silicon substrate by MOCVD. The detailed description of the CVD apparatus can be found elsewhere (Xiong et al. [2006]). The measured reflectance at 950 nm and 470 nm is shown in Fig. 4. The time interval between consecutive peaks at 470 nm are 39.6, 41.3, 44.2, 47.8, 52.0, 50.9 minutes. This indicated that growth rate is gradually decreasing.

We first use RLS to extract thickness, roughness and refractive indices. Initially $x_1 = [0 \quad 2.7 \quad 0 \quad 0.5 \quad 2 \quad 2]^T$. According to Palik and Ghosh [1998], the refractive index of yttrium oxide at room temperature is 1.9054 and 1.9455

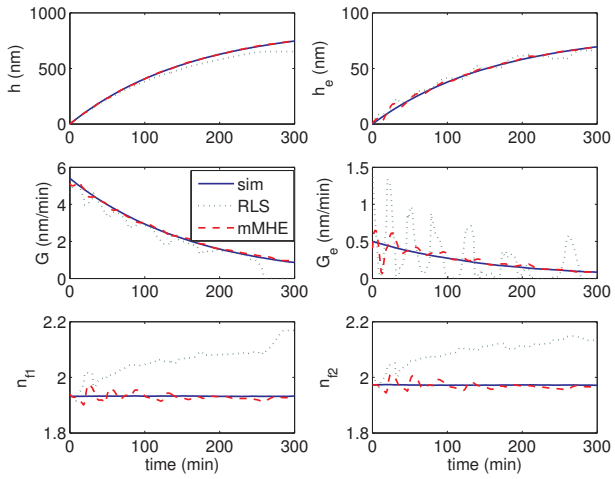

Fig. 2. Comparison between simulated states by RLS and mMHE with window size equal to 10.

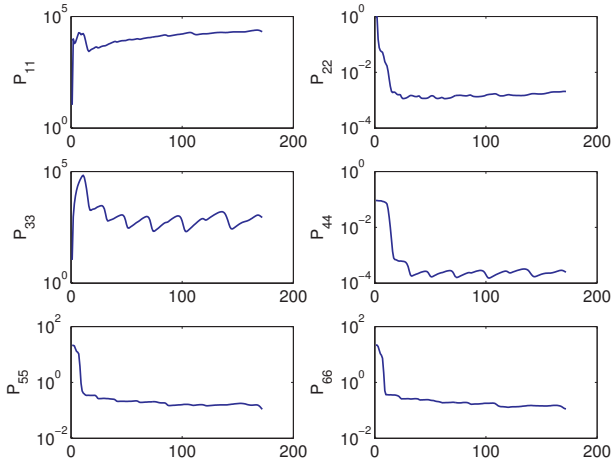

Fig. 3. Evolution of covariance matrix in mMHE.

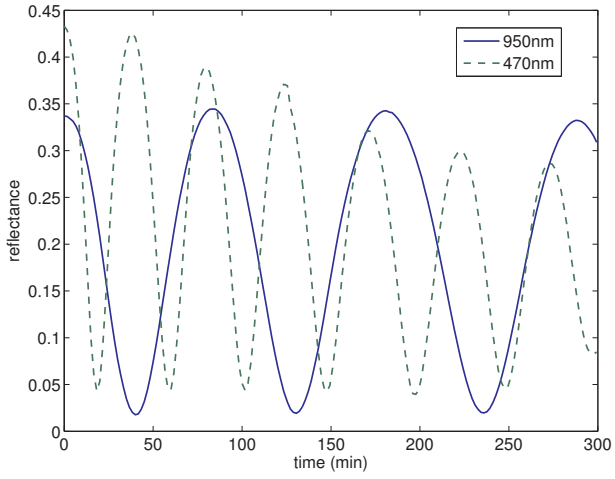

Fig. 4. *In situ* reflectance signal during deposition of yttria polycrystalline film on a silicon substrate.

for 950 nm and 470 nm, respectively. This CVD experiment was carried out at approximately 650 °C. Refractive indices of oxides usually increase with temperature. Therefore we chose 2 as the initial guess for the refractive indices. The initial guess of the growth rate was estimated from

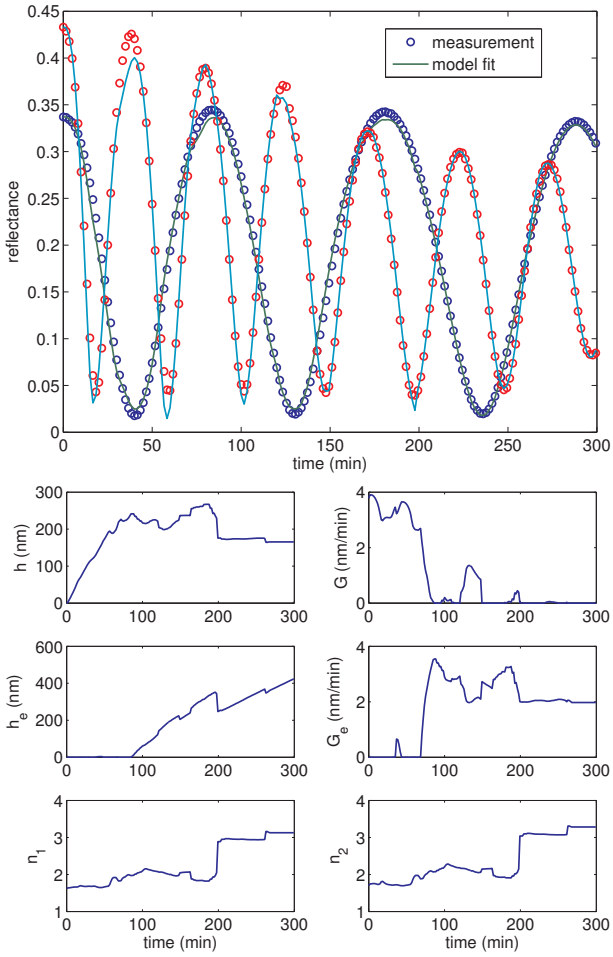

Fig. 5. Estimation result by RLS. (top) measurement (bottom) states

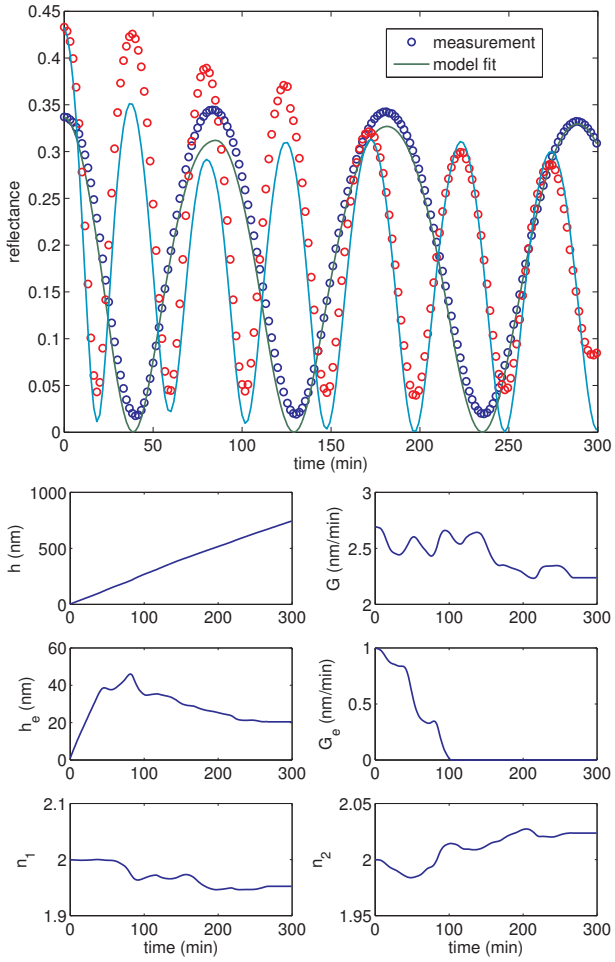

Fig. 6. Estimation result by mMHE. (top) measurement (bottom) states

previous experiments and is a typical average value. Because the sensor model is highly nonlinear, it is important to have a good initial guess to start. Positive constraints were applied to all states. The window size was chosen to be 20 which corresponds to almost half oscillation for 470 nm reflectance and a quarter oscillation for 950 nm (Breiland and Killeen [1995]). The time interval is 100 seconds. Figure 5 shows the estimation results by RLS. As shown, although the measurement was fitted pretty well, the estimated states are not physically reasonable. This suggested that without considering the *a priori* knowledge of the parameters, the fitting algorithm tends to overfit the measurement data because the parameters are highly correlated. In addition, the objective function in RLS consists only the sensor model error. But in reality the sensor model will not be perfectly accurate. For example, in the experiment there will be slight calibration error and film nonuniformity, which may be causing the large reflectance values in the valleys. Further unmodeled effects include film porosity. Therefore to only fit to an imperfect sensor model could lead to very poor estimates.

On the other hand, mMHE allows more control over the fit by including the *a priori* estimate and the estimated uncertainty in the objective function. The initial covariance matrices are $P_{1|0} = \text{diag}(x_1 \times 0.1) \times 10^{-2}$, $Q = \text{diag}(x_1 \times 0.1) \times 10^{-2}$ and $R = \text{eye}(2)$. Notice that P_1 is smaller and R is larger than in the simulation study. This is because the sensor model in the experimental study is not perfect like in the simulation study. Therefore we need to increase R to indicate less confidence on the sensor model and decrease P_1 to indicate a good starting point for the fit. With the same initial guess and a window size of 20, the estimation result by mMHE is shown in Fig. 6. The estimated states become much smoother due to the inclusion of the *a priori* estimate. The measurements are not fitted perfectly like in Fig. 5. This is expected because the sensor model is not perfect so the mMHE weighted less on the sensor model. The estimated final film thickness is 742 nm. The estimated refractive indices are 1.96 and 2.03 for 950 nm and 470 nm, respectively. We used an ellipsometer to measure film thickness and refractive indices *ex situ*. The film thickness is 722 nm. The refractive indices are 1.92 and 1.96 for 950 nm and 470 nm, respectively. The estimated film thickness is only 2.7% offset from the *ex situ* measurement which indicates a very reasonable estimate. The estimated refractive indices are slightly larger than the *ex situ* measurements. The *ex situ* ellipsometry was carried out at room temperature and the CVD was carried out at high temperature. Considering temperature difference, the estimated refractive indices are reasonable because the refractive index of metal oxide usually increases with temperature. In fact this method could be used to measure the refractive indices of metal

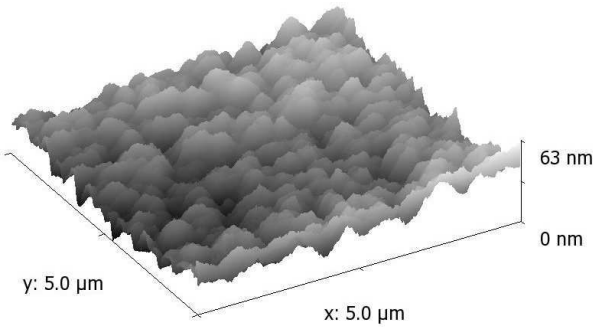

Fig. 7. AFM image of the deposited film

oxides at high temperature. For the surface roughness, we used AFM to measure the surface profile. Figure 7 shows the AFM image at a scan size of 5 micron. The RMS roughness is reported to be 7 nm. The estimated final effective layer thickness is 20 nm. According to Carniglia and Jensen [2002], the RMS roughness σ and the effective layer thickness d is related by $\sigma = d/2 = 10$ nm. The factor of 2 is needed because the EMA thickness is peak-to-peak, while the AFM value is only root-mean-square. Therefore the roughness estimated by mMHE falls into a reasonable range when considering the roughness reported by AFM.

5. CONCLUSION

In this paper we proposed a modified moving horizon estimator (mMHE) to extract film microstructure from *in situ* reflectance measurements. mMHE assumes a deterministic process model to improve computation efficiency and includes the *a priori* estimate in the objective function. It also uses the extended Kalman filter to update the *a priori* estimate and covariance. mMHE was compared with RLS in both simulated and experimental CVD processes. The results indicated that mMHE yielded more accurate estimates by utilizing the *a priori* estimate. We have applied mMHE to interpret *in situ* reflectance data but the same technique can be used for other optical sensors which face similar issues in data interpretation such as the ellipsometer. Currently optical sensors with RLS estimation have only limited applicability in ideal systems like ultra-high vacuum molecular beam epitaxy. But with a more robust estimation method, optical sensors could have wider applicability, such as in CVD, enabling the greater use of feedback control.

REFERENCES

R. S. Balmer, C. Pickering, A. J. Pidduck, and T. Martin. Modelling of high temperature optical constants and surface roughness evolution during MOVPE growth of GaN using *in situ* spectral reflectometry. *Journal of Crystal Growth*, 245(3-4):198–206, November 2002.

W. G. Breiland and K. P. Killeen. A virtual interface method for extracting growth rates and high temperature optical constants from thin semiconductor films using *in situ* normal incidence reflectance. *Journal of Applied Physics*, 78(11):6726–6736, 1995.

C. Buzea and K. Robbie. State of the art in thin film thickness and deposition rate monitoring sensors. *Reports on Progress in Physics*, 68(2):385–409, 2005.

C. K. Carniglia and D. G. Jensen. Single-layer model for surface roughness. *Applied Optics*, 41(16):3167–71, 2002.

G. Comina, J. Rodriguez, J. L. Solis, and W. Estrada. *In situ* laser reflectometry measurements of pyrolytic ZnO film growth. *Measurement Science & Technology*, 16(3): 685–690, March 2005.

A. W. Crook. The reflection and transmission of light by any system of parallel isotropic films. *Journal of the Optical Society of America*, 38(11):954–964, 1948.

E. L. Haseltine and J. B. Rawlings. Critical evaluation of extended kalman filtering and moving-horizon estimation. *Industrial & Engineering Chemistry Research*, 44 (8):2451–2460, April 2005.

G. E. Jellison and H. H. Burke. The temperature dependence of the refractive index of silicon at elevated temperatures at several laser wavelengths. *Journal of Applied Physics*, 60(2):841–843, 1986.

G. E. Jellison and F. A. Modine. Optical functions of silicon at elevated temperatures. *Journal of Applied Physics*, 76(6):3758–3761, 1994.

J. L. Luo, X. T. Ying, P. N. Wang, and L. Y. Chen. Study on the growth of CVD diamond thin films by *in situ* reflectivity measurement. *Diamond and Related Materials*, 11:1871–1875, 2002.

Edward D. Palik and Gorachand Read Ghosh. *Handbook of optical constants of solids*. Academic Press, San Diego, 1998.

Hugh O. Pierson. *Handbook of chemical vapor deposition (CVD): principles, technology, and applications*. Noyes Publications/William Andrew Pub., Norwich, N.Y., 2nd edition, 1999.

C. V. Rao, J. B. Rawlings, and J. H. Lee. Constrained linear state estimationa moving horizon approach. *Automatica*, 37(10):1619–1628, October 2001.

C. V. Rao, J. B. Rawlings, and D. Q. Mayne. Constrained state estimation for nonlinear discrete-time systems: Stability and moving horizon approximations. *IEEE Transaction on Automatic Control*, 48(2):246–258, February 2003.

D. G. Robertson and J. H. Lee. A least-squares formulation for state estimation. *Journal of Process Control*, 5 (4):291–299, August 1995.

D. G. Robertson, J. H. Lee, and J. B. Rawlings. A moving horizon-based approach for least-squares estimation. *AICHE Journal*, 42(8):2209–2224, August 1996.

A. Stafford, S. J. C. Irvine, K. L. Hess, and J. Bajaj. The use of *in situ* laser interferometry for MOCVD process control. *Semiconductor Science and Technology*, 13(12): 1407–1411, December 1998.

R. T. Xiong and M. A. Gallivan. Moving horizon estimation for *in situ* monitoring of chemical vapor deposition process. In *Proceedings of the American Control Conference*, New York, July 2007.

R. T. Xiong, P. J. Wissmann, and M. A. Gallivan. An extended Kalman filter for *in situ* sensing of yttria-stabilized zirconia in chemical vapor deposition. *Computers and Chemical Engineering*, 30:1657–1669, 2006.

C. D. Zuiker, D. M. Gruen, and A. R. Krauss. In situ laser reflectance interferometry measurement of diamond film growth. *Journal of Applied Physics*, 79:3541–3547, 1996.